Dietary restriction and clock delay eye aging to extend lifespan in D. melanogaster

Brian Hodge (bhodge@buckinstitute.org)
Buck Institute for Research on Aging https://orcid.org/0000-0001-6190-9363
Geoffrey Meyerhof
University of California, Santa Barbara
Subhash Katewa
NGM Biopharmaceuticals
Ting Lian
Sichuan Agricultural University
Charles Lau
Buck Institute for Research on Aging
Sudipta Bar
Buck Institute for Research on Aging
Nicole Leung
Stanford University
Menglin Li
University of California, Santa Barbara
David Li-Kroeger
Baylor College of Medicine https://orcid.org/0000-0001-6473-7691
Simon Melov
Buck Institute for Research on Aging https://orcid.org/0000-0001-8554-2834
Birgit Schilling
Buck Institute for Research on Aging https://orcid.org/0000-0001-9907-2749
Craig Montell
UC Santa Barbara https://orcid.org/0000-0001-5637-1482
Pankaj Kapahi
Buck Institute for Research on Aging

Article

Keywords: Circadian Regulation, Visual System, Visual Senescence, Systemic Immune Response, Photoreceptor Activation, Organismal Aging

Posted Date: May 21st, 2021

DOI: https://doi.org/10.21203/rs.3.rs-428198/v1

Version of Record: A version of this preprint was published at Nature Communications on June 7th, 2022.
See the published version at https://doi.org/10.1038/s41467-022-30975-4.

Dietary restriction and *clock* delay eye aging to extend lifespan in *D. melanogaster*

Brian A. Hodge[1*], Geoffrey T. Meyerhof[1,4], Subhash D. Katewa[1,2], Ting Lian[1,3], Charles Lau[1], Sudipta Bar[1], Nicole Leung[4,5], Menglin Li[4], David Li-Kroeger[6], Simon Melov[1], Birgit Schilling[1], Craig Montell[4], Pankaj Kapahi[1*]

[1]Buck Institute for Research on Aging, 8001 Redwood Blvd, Novato, CA 94945, USA.

[2]NGM Biopharmaceuticals, 333 Oyster Point Blvd, South San Francisco, CA 94080, USA.

[3]Sichuan Agricultural University, 46 Xinkang Rd, Yucheng District, Ya'an, Sichuan, China.

[4]Neuroscience Research Institute and Department of Molecular, Cellular and Developmental Biology, University of California, Santa Barbara, Santa Barbara, 93106, California, USA.

[5]Department of Psychiatry and Behavioral Sciences, Stanford University, Stanford, CA 94305, USA; Department of Neurobiology, Stanford University, Stanford, CA 94305, USA.

[6]Department of Neurology, Baylor College of Medicine, Houston, TX 77096, USA.

*Correspondence: bhodge@buckinstitute.org, pkapahi@buckinstitute.org

Abstract

Many vital processes in the eye are under circadian regulation, and circadian dysfunction has emerged as a potential driver of eye aging. Dietary restriction is one of the most robust lifespan-extending therapies and amplifies circadian rhythms with age. Herein, we demonstrate that dietary restriction extends lifespan in *D. melanogaster* by promoting circadian homoeostatic processes that protect the visual system from age- and light-associated damage. Disrupting circadian rhythms in the eye by inhibiting the transcription factor, Clock (CLK), or CLK-output genes, accelerated visual senescence, induced a systemic immune response, and shortened lifespan. Flies subjected to dietary restriction were protected from the lifespan-shortening effects of photoreceptor activation. Inversely, photoreceptor inactivation, achieved via mutating rhodopsin or housing flies in constant darkness, primarily extended lifespan in flies reared on a high-nutrient diet. Our findings establish the eye as a diet-sensitive modulator of lifespan and indicate that vision is an antagonistically pleiotropic process that contributes to organismal aging.

Introduction

Circadian rhythms are approximate 24-hour oscillations in behavior, cellular physiology, and biochemistry, which evolved to anticipate and manage predictable changes associated with the solar day (e.g., predator/prey interactions, nutrient availability, phototoxicity, etc.) [1]. Circadian rhythms are generated by endogenous clocks that sense time-cues (e.g., light and food) to govern rhythmic oscillations of gene transcriptional programs, synchronizing cellular physiology with daily environmental stressors [2]. In addition to keeping time, the molecular clock regulates the temporal expression of downstream genes, known as clock-controlled genes, to promote tissue-specific rhythms in physiology [3]. The *Drosophila* molecular clock is comprised of transcriptional-translational feedback loops, where the transcription factors Clock (CLK) and Cycle (CYC) rhythmically activate their own repressors, Period and Timeless [2]. This feedback loop not

only exists in central pacemaker neurons, where it sets rhythms in locomotor activity, it also functions in peripheral tissues, such as the eye [4].

Aging is associated with a progressive decline in visual function and an increase in the incidence of ocular disease. *Drosophila* photoreceptor cells serve as a powerful model of both visual senescence and retinal degeneration [5, 6]. *Drosophila* and mammalian photoreceptors possess a cell-intrinsic molecular clock mechanism that temporally regulates a large number of physiological processes, including light-sensitivity, metabolism, pigment production, and susceptibility to light-mediated damage [7]. Visual senescence is accompanied by a reduced circadian amplitude in core-clock gene expression within the retina [8]. This reduction in retinal circadian rhythms may be causal in eye aging, as mice harboring mutations in their core-clock genes, either throughout their entire body, or just in their photoreceptor cells, display several early-onset aging phenotypes within the eye. These mice prematurely form cataracts and have reduced photoreceptor cell light-sensitivity and viability [8]. However, the molecular mechanisms by which the molecular clock influences eye aging are not fully understood.

Dietary restriction (DR), defined by reducing specific nutrients or total calories, is the most robust mechanism for delaying disease and extending lifespan [9]. The mechanisms by which DR promotes health and lifespan may be integrally linked with circadian function, as DR enhances the circadian transcriptional output of the molecular clock and preserves circadian function with age [10]. Inversely, high-nutrient diets (i.e.,

excess consumption of protein, fats, or total calories) repress circadian rhythms and accelerate organismal aging [11, 12]. However, how DR modulates circadian rhythms within the eye, and how these rhythms influence DR-mediated lifespan extension, had yet to be examined.

Herein, we sought to elucidate the circadian processes that are activated by DR by performing an unbiased, 24-hour time-course mRNA expression analysis in whole flies. We found that circadian processes within the eye are highly elevated in expression in flies reared on DR. In particular, DR enhanced the rhythmic expression of genes involved in the adaptation to light (i.e., calcium handling and de-activation of rhodopsin-mediated signaling). Building on this observation, we demonstrate that the majority of these circadian phototransduction components were transcriptionally regulated by CLK. Eliminating CLK function either pan-neuronally, or just in the photoreceptors, accelerated visual decline with age. Furthermore, disrupting photoreceptor homeostasis increased systemic immune responses and shortened lifespan. Several eye-specific CLK-output genes that were upregulated in expression in response to DR, were also required for DR- to slow visual senescence and extend lifespan.

Results

99 *Dietary restriction amplifies circadian transcriptional output and delays visual senescence*
100 *in a CLK-dependent manner*
101 To determine how DR changes circadian transcriptional output, we performed a series of
102 microarray experiments over the span of 24-hours in female *Canton-S* flies (whole body)
103 reared on either a high-yeast (5%; *ad libitum*, AL) diet or a low-yeast (0.5%; DR) diet
104 (**Supplementary Fig. 1a**). Flies maintained on DR displayed nearly twice the number
105 circadian transcripts compared to flies on AL (**Fig. 1a, b and Supplementary Fig. 1b**).
106 Circadian gene expression was also more robust on DR vs AL. DR-specific oscillators were
107 statistically more rhythmic (lower JTK_CYCLE circadian *p*-values) and displayed larger
108 circadian amplitudes than AL-specific oscillators (**Supplementary Fig. 1c, d**). Diet also
109 drastically altered the circadian transcriptional profile, as only 16% of DR oscillators were
110 also oscillating on AL (**Supplementary Fig. 1b**). Furthermore, the AL and DR circadian
111 transcriptomes were enriched for distinct processes (**Supplementary Fig. 1e, f and**
112 **Supplementary Data 1**).
113 Transcripts that oscillate on both AL and DR diets were highly enriched for genes
114 that comprise the canonical phototransduction signaling cascade (**Fig. 1c-d**), which is the
115 process by which *Drosophila* photoreceptor cells, the primary light-sensitive neurons,
116 transduce light information into a chemical signal [13]. Briefly, light-mediated conversion
117 of rhodopsin proteins to their meta-rhodopsin state stimulates heterotrimeric Gq proteins
118 that activate phospholipase C (*norpA*), which produces secondary messengers and

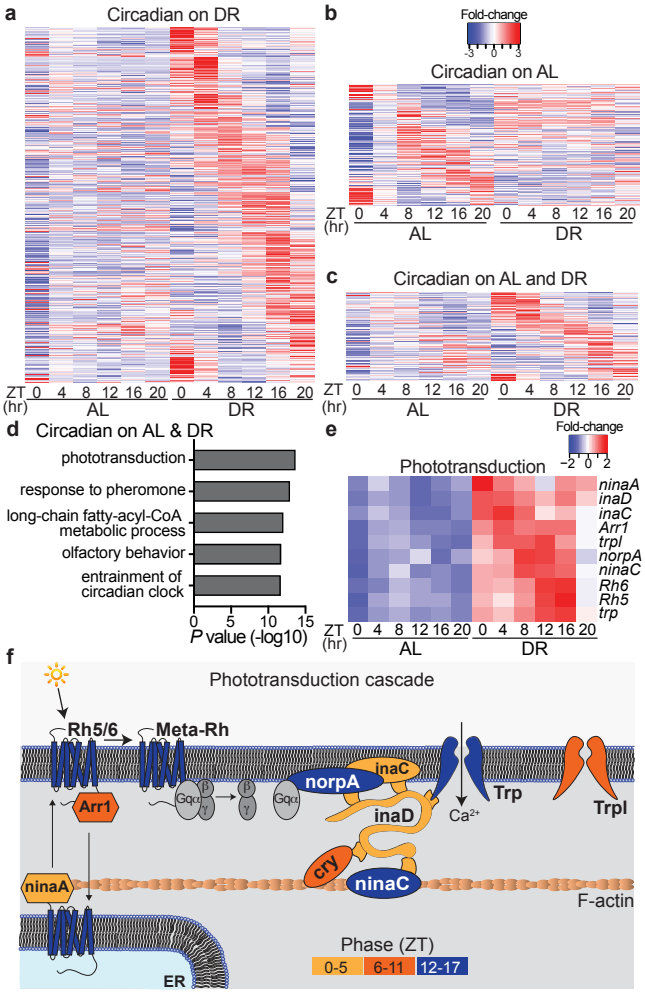

Figure 1. Dietary restriction amplifies circadian transcriptional output and rhythmicity of phototransduction genes. (**a-c**) Circadian transcriptome heatmaps for Canton-S flies representing 24-hour expression plots for transcripts that cycle only on DR (a, *n*=1609 transcripts), only on AL (b, *n*=568 transcripts), or on both diets (c, *n*=301 transcripts). Circadian transcripts (24h period, JTK_CYCLE *p*value<0.05) are plotted by phase. (**d**) Gene-ontology enrichment categories corresponding to transcripts that cycle on both AL and DR diets. (**e**) Heatmap of phototransduction transcript expression on AL and DR. (**f**) Phototransduction cascade diagram with components colored according to their circadian phase on DR.

promotes the opening of Transient Receptor Potential channels (TRP, TRPL), ultimately allowing Ca^{2+} and Na^{+} to depolarize the photoreceptor cell [14]. Although the phototransduction transcripts were cyclic on both diets, on DR their expression became more rhythmic (lower JTK_CYCLE *p*-values & larger circadian amplitudes) and elevated (~2-fold increase in expression across all timepoints) (**Fig. 1e and Supplementary Fig. 1i**). Since our time-course analyses were perfromed in whole-fly, we queried publicly available circadian transcriptomes from wild-type heads to further investigate the rhythmic oscillations of eye-related transcripts [15]. The majority of the DR-sensitive phototransduction genes also robustly cycled in wild-type heads (**Supplementary Table 1**). Furthermore, the GO-term "phototransduction" (GO:0007602) was amongst the most enriched cyclic processes in the heads of wild-type flies, as ~70% of the genes that comprise the category oscillate in a circadian fashion (**Supplemental Data 2**).

In *Drosophila* and mammals, visual function oscillates to align with daily changes in ambient illuminance from the sun, which can be 10^6 to 10^8-fold brighter during the day than at night [16]. Photoreceptors are unique in that they have evolved mechanisms responsible for maintaining homeostasis in the presence of light-induced calcium ion gradients that are magnitudes greater than what other neuronal populations experience [17, 18]. Mechanisms of light adaptation within photoreceptors include the rapid (millisecond) closure of TRP channels (facilitated via enzymes scaffolded by *inaD*), rhodopsin internalization from the rhabdomere membrane (e.g., *arr1*, *arr2*), and calcium

efflux (e.g., *calx*) [19, 20]. Acrophase analyses (i.e., time of peak expression) revealed that circadian transcripts that promote photoreceptor activation (Ca^{2+} influx) reach peak expression during the dark-phase, while genes that terminate the phototransduction response (i.e., deactivation of rhodopsin mediated signaling) peak in anticipation of the light-phase (**Fig. 1f and Supplementary Fig. 1j**). These findings provide a potential mechanistic explanation for the rhythmic response pattern in light-sensitivity observed in *Drosophila* photoreceptors and suggests that DR's ability to delay visual senescence is mediated in part by amplifying circadian rhythms within photoceptors (See **Supplemental Discussion 1** for additional interpretations).

To determine if molecular clocks mediate the enhanced rhythmic expression of phototransduction genes on DR, we measured the transcriptome of fly heads with pan-neuronal over-expression of a dominant negative form of the core-clock factor, CLK (Elav-GS-GAL4>UAS-CLK-Δ1; denoted nCLK-Δ1) (**Supplementary Fig. 2a**). To avoid potential developmental defects related to Clk disruption, we used a drug-inducible (RU486) "gene-switch" driver to express CLK-Δ in adult flies. Genes downregulated in nCLK-Δ1 heads were enriched for light-response pathways, including "response to light stimulus" and "deactivation of rhodopsin signaling" (**Fig. 2a, b and Supplemental Data 3**). Additionally, genes that were both circadian in wild-type heads and downregulated in nCLK-Δ1 were highly enriched for homeostatic processes related to eye function (**Supplementary Fig. 2c**

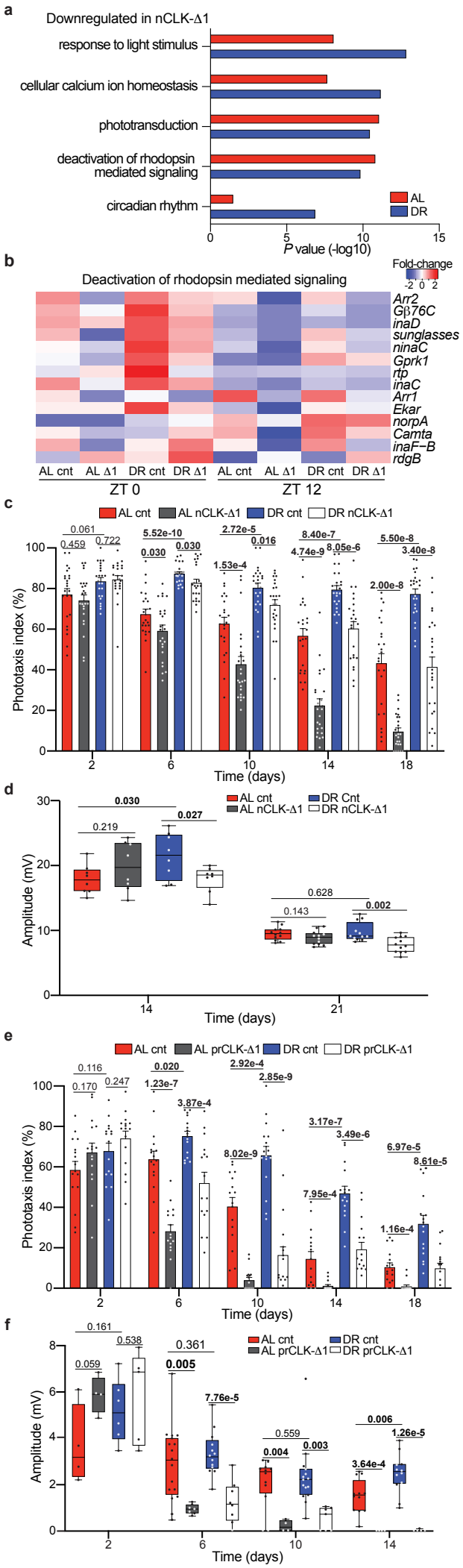

Figure 2. Dietary restriction delays visual senescence in a CLK-dependent manner. (**a**) GO enrichment scores corresponding to downregulated light-response genes in heads from RNA-Seq of nCLK-Δ1 (Elav-GS-GAL4> UAS-CLK-Δ1) vs controls. (**b**) Heatmap of normalized RNA-Seq expression corresponding to the gene-ontology category "Deactivation of rhodopsin mediated signaling" (GO:0016059) in nCLK-Δ1 and controls at zeitgeber times 0 and 12 (lights on and lights off, respectively). (**c**) Positive phototaxis responses for nCLK-Δ1 flies. For each timepoint results are represented as average percent positive phototaxis +/- SEM (n=24 biological replicates, N=480 flies per condition). (**d**) Boxplots of electroretinogram amplitudes for nCLK-Δ1 flies and controls at day 14 and 21. (**e**) Positive phototaxis responses for prCLK-Δ1 flies (Trpl-GAL4; GAL80^{ts}> UAS-CLK-Δ1) and control flies (Trpl-GAL4; GAL80^{ts}>*CantonS*) reared at 30°C. For each timepoint results are represented as average percent positive phototaxis +/- SEM (n=16 biological replicates, N=320 flies per condition). (**f**) Boxplots of electroretinogram amplitudes for prCLK-Δ1 and control flies reared at 30°C. Illuminance was set at 150 Lux. (c-f) Pvalues were determined by two-tailed Student's $t$test (unpaired), comparing responses between diet and/or genotype at each timepoint.

158 **and Supplemental Data 4**). Together, this indicates that CLK governs the circadian
159 transcriptional regulation of many eye-related processes in *Drosophila*.

160 Given DR's ability to improve homeostasis across an array of tissues [21], and its
161 ability to enhance the circadian rhythmicity of light-response genes, we examined how
162 diet and clocks influence visual function with age. We longitudinally quantified the
163 positive phototaxis response of wild-type flies (*Canton-S* and *Oregon-R*) reared on either
164 AL or DR diets (experimental setup in Supplementary Fig. 2d). Compared to AL-fed flies,
165 DR slowed the decline in positive phototaxis observed with age (**Supplementary Fig. 2e,**
166 **f**). Importantly, this effect cannot solely be attributed to diet-dependent changes in
167 locomotor activity, as climbing activity and phototaxis declined at different rates with age
168 (**Supplementary Fig. 2g**). Compared to wild-type flies, DR minimally protected Clk^{out} (*Clk*-
169 null) flies from age-related declines in phototaxis (**Supplementary Fig. 2h**). nCLK-Δ1 and
170 nCLK-Δ2 (an additional dominant negative *Clk* mutant, Elav-GS-GAL4>UAS-CLK-Δ2) flies
171 displayed accelerated declines in positive phototaxis with age compared to controls (**Fig.**
172 **2c and Supplementary Fig. 2i**). Since the positive phototaxis assay measures a behavioral
173 response to light, we next evaluated how diet and CLK directly influence photoreceptor
174 function with age by performing extracellular electrophysiological recordings of the eye
175 (electroretinograms, ERG [22]). We observed larger ERG amplitudes, i.e. the light-induced
176 summation of receptor potentials from the photoreceptors [23], in control flies reared on

177 DR vs AL at day 14 (**Fig. 2d**). Furthermore, the DR-mediated enhancements in the ERG
178 amplitudes were significantly reduced in nCLK-Δ1 flies with age (**Fig. 2d**).

179 Since the Elav-GS-GAL4 driver is expressed in a pan-neuronal fashion (i.e.,
180 photoreceptors + extra-ocular neurons), we sought to examine how disrupting CLK
181 function solely within photoreceptors influences visual function with age. To this end, we
182 crossed UAS-CLK-Δ1 flies with a photoreceptor-specific GAL4 driver line under the
183 temporal control of the temperature sensitive GAL80 protein (Trpl-GAL4; $GAL80^{ts}$>UAS-
184 CLK-Δ1, denoted prCLK-Δ1). To avoid disrupting CLK function during development,
185 prCLK-Δ1 flies were raised at 18°C (GAL80 active, GAL4 repressed) and then transferred
186 to 30°C (GAL80 repressed, GAL4 active) following eclosion. When compared to control
187 flies (Trpl-GAL4; $GAL80^{ts}$>*CantonS*), prCLK-Δ1 flies displayed accelerated declines in both
188 positive phototaxis and ERG amplitude with age, and in a similar fashion to the nCLK-Δ1
189 flies (**Fig. 2e-f**). Together, our gene expression, phototaxis, and ERG data indicate that DR
190 functions in a CLK-dependent manner to delay photoreceptor aging in the fly.

191 ***nCLK-Δ drives a systemic immune response and reduces longevity***

192 Age-related declines in tissue homeostasis are accompanied by elevated immune
193 responses and inflammation [24, 25]. Interestingly, we found that genes upregulated in
194 nCLK-Δ1 fly heads were significantly enriched for immune and antimicrobial humoral
195 responses (**Fig. 3a, b**). In *Drosophila,* damage-associated molecular patterns can induce a
196 sterile immune response that is characterized by the expression of anti-microbial peptides

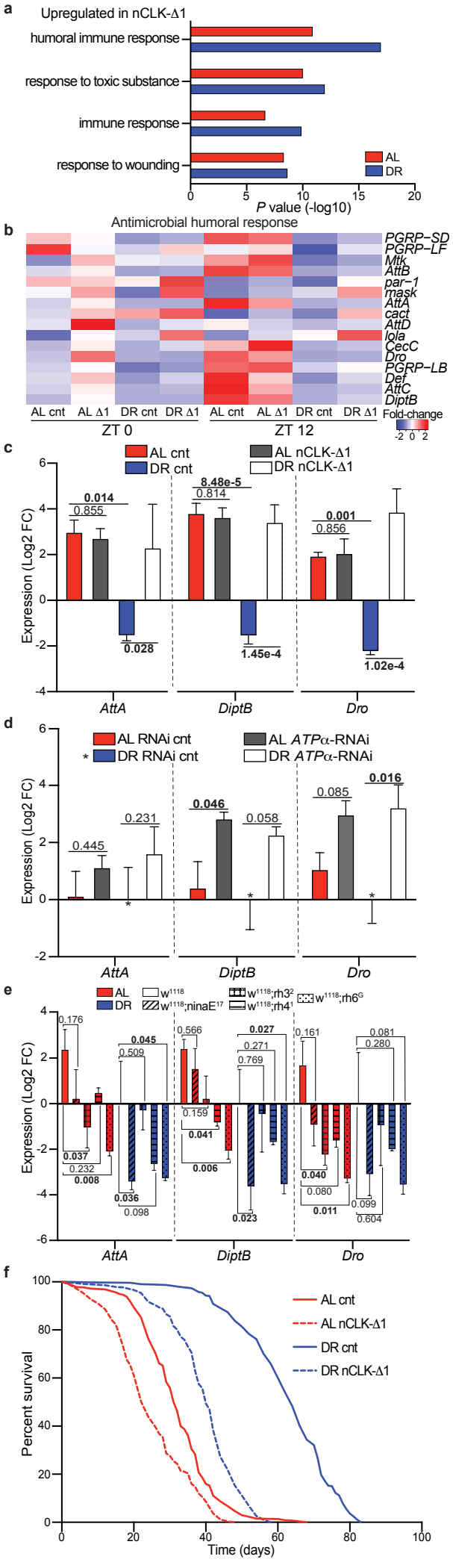

Figure 3. nCLK-Δ1 flies display elevated immune responses and shortened lifespan. (**a**) GO enrichment scores corresponding to upregulated inflammatory genes in heads from RNA-Seq of nCLK-Δ1 vs controls. (**b**) Heatmap of normalized RNA-Seq expression corresponding to the gene-ontology category "Antimicrobial humoral responses" (GO:0019730) in nCLK-Δ1 and controls. (**c**) Relative expression of AMP genes (*AttA*, *DiptB*, and *Dro*) calculated by RT-qPCR with mRNA isolated from nCLK-Δ1 bodies. Results are plotted as average Log2 fold-change in expression calculated by the ΔΔ-Ct method, normalized to DR vehicle treated control samples, as well as the housekeeping gene *rp49* +/- SEM (*n*=3 biological replicates, *N*=30 flies per biological replicate). (**d**) Relative mRNA expression of AMP genes calculated by RT-qPCR with mRNA isolated from bodies of eye-specific *ATPα* knockdown flies (GMR-GAL4>UAS-*ATPα*-RNAi) vs RNAi control flies (GMR-GAL4>UAS-*mCherry*-RNAi). Results are plotted as average Log2 fold-change in expression calculated by the ΔΔ-Ct method, normalized to DR RNAi control samples as well as housekeeping gene *rp49* +/- SEM (*n*=3 biological replicates, *N*=30 flies per biological replicate). (**e**) Relative mRNA expression of immune genes (*AttaA*, *DiptB*, and *Dro*) calculated by RT-qPCR with mRNA isolated from bodies of w1118 and rhodopsin mutant flies housed in 12:12h LD. Results are plotted as average Log2 fold-change in expression calculated by the ΔΔ-Ct method normalized w^{1118} DR control samples as well as *rp49* +/- SEM (*n*=3 biological replicates, *N*=30 flies per biological replicate). (**f**) Kaplan-Meyer survival analysis of nCLK-Δ1 flies (Elav-GS-GAL4>UAS-CLK-Δ1). Survival data is plotted as an average of three independent lifespan repeats. Control flies (vehicle treated): AL *N*=575, DR *N*=526; nCLK-Δ1 flies (RU486 treated): AL *N*=570, DR *N*=565. (c-e) *P*values were calculated with the pairwise Student's *t*test comparing Log2 fold-changes in expression.

197 (AMPs), similar to the effects from infections by pathogens [26]. We quantified the mRNA
198 expression of AMPs in the bodies of nCLK-Δ1 and nCLK-Δ2 flies to determine if neuronal
199 damage signals propagate throughout the body to drive systemic immune responses; the
200 *Drosophila* fat body generates high levels of AMPs in response to intrinsic damage signals
201 [26]. AMP expression (*AttA*, *DiptB*, and *Dro*) was reduced in control flies reared on DR
202 compared to AL, however nCLK-Δ1 and nCLK-Δ2 elevated AMP expression on DR (**Fig. 3c**
203 **and Supplementary Fig. 3a**). To further investigate this systemic inflammatory response,
204 we isolated and quantified hemolymph from nCLK-Δ1 and control flies. In agreement with
205 the transcriptional activation of AMPs in both the heads and bodies of nCLK-Δ1 flies, we
206 found the most highly upregulated protein in nCLK-Δ1 hemolymph to be the
207 antimicrobial peptide, AttC (**Supplementary Fig. 3b**). Furthermore, we observed an
208 enrichment for proteins associated with translational activation (e.g., cytoplasmic
209 translation and ribosomal biogenesis) within the upregulated proteins in the nCLK-Δ1
210 hemolymph, which may reflect the activation of hemocytes, the immune effector cells in
211 *Drosophila* (**Supplemental Data 5**) [27]. Taken together, these data demonstrate that
212 disrupting neuronal CLK function elevates systemic immune responses.
213 To determine if photoreceptor degeneration induces a systemic immune response
214 in *Drosophila*, we forced photoreceptor degeneration by knocking down *ATPα* within the
215 eye (GMR-GAL4>UAS-*ATPα*-RNAi), and quantified expression of AMPs within the bodies.
216 *ATPα* encodes the catalytic alpha subunit of the Na^+K^+ATPase responsible for

reestablishing ion balance in the eye during light responses [28, 29]. Our decision to use *ATPα* knockdown as a model of photoreceptor degeneration was motivated by previous reports indicating that its expression is under circadian regulation [30] and that its knockdown in the eye results in aberrant ion homeostasis that drives age-dependent, light-independent photoreceptor degeneration [31]. Ocular knockdown of *ATPα* rendered flies blind in both AL and DR conditions compared to controls (**Supplementary Fig. 3c**). Knocking down *ATPα* in the eye also drove the expression of AMPs within the bodies of flies reared on either an AL or DR diet (**Fig. 3d**). Thus, DR fails to suppress immune responses in the context of forced photoreceptor degeneration.

Since we found that photoreceptor degeneration induced systemic immune responses, we postulated that reducing phototransduction should reduce inflammation. To assess how stress from environmental lighting influences immune responses, we analyzed a circadian microarray dataset comparing gene expression changes in wild-type (*y,w*) heads in flies reared in 12hr light and 12hr darkness (12:12LD) or constant darkness [32]. We found immune response genes to be among the most highly enriched processes upregulated in the flies housed in 12:12LD vs constant darkness (**Supplementary Fig. 3d, e and Supplemental Data 8**). We quantified AMPs within the bodies of flies harboring rhodopsin null mutations to evaluate how the different photoreceptor subtypes influence systemic immune responses. The *Drosophila* ommatidia consists of eight photoreceptors (R1-8) that express different rhodopsins with varying sensitives to distinct wavelengths of

light [33]. The R1-6 photoreceptors express the major rhodopsin Rh1, encoded by *ninaE*, while the R7 photoreceptor expresses either Rh3 or Rh4. The R8 photoreceptor expresses either Rh5 or Rh6 [34]. The rhodopsin null mutants [*ninaE* [35], *rh3* [36], *rh4* [37] , or *rh6* [38]] displayed reductions in immune marker expression in their bodies compared to w^{1118} outcrossed controls (**Fig. 3e**). Taken together, these findings indicate that suppression of rhodopsin mediated signaling is sufficient to suppress systemic immune responses in *Drosophila*.

Given the strong associations between chronic immune activation and accelerated aging, we examined the lifespans of nCLK-Δ flies [24]. Both nCLK-Δ1 and nCLK-Δ2 flies displayed significantly shortened lifespans, with a proportionally greater loss in median lifespan in flies reared on DR compared to AL (**Fig. 3f and Supplementary Fig. 3f-h**). nCLK-Δ flies have altered CLK function throughout all neurons, however, it is possible that the lifespan-shortening effect observed in these lines was substantially driven by loss of CLK-function within the eye; Others have demonstrated that CLK is highly enriched (>5-fold) within photoreceptors compared to other neuronal cell types in *Drosophila* (**Supplementary Fig. 3i**) [5]. Furthermore, over-expressing CLK-Δ1 within just photoreceptors (prCLK-Δ1) also shortened lifespan (**Supplementary Fig. 3j**). These findings argue that neuronal CLK function is required for the full lifespan extension mediated by DR and indicate that photoreceptor clocks are essential for maintenance of visual function with age and organismal survival.

DR protects against lifespan shortening from photoreceptor cell stress

Previous reports have demonstrated that exposure to light can decrease lifespan—extending the daily photoperiod, or housing flies in blue light reduces longevity [39, 40]. Since DR delays visual senescence and promotes the rhythmic expression of genes involved in photoreceptor homeostasis (i.e., light adaptation, calcium handling), we investigated how diet influences survival in the context of light and/or phototransduction. To test the interrelationship among diet, light, and survival, we housed w^{1118} (white-eyed) in either a 12:12 LD cycle or constant darkness. Housing flies in constant darkness extended the lifespan of flies reared on AL, while the lifespans of flies reared on DR were unaffected (**Fig. 4a**). Constant darkness failed to extend the lifespan of red-eyed (w^{+}) *Canton-S* wild-type flies (**Supplementary Fig. 4a**), suggesting that the ATP-binding cassette transporter encoded by *w,* and the red-pigment within the cone-cells, helps to protect against lifespan shortening from diet- and light-mediated stress [41]. White-eyed, photoreceptor null flies (homozygous for TRP^{P365} mutation [42]) reared on AL failed to display lifespan extension in constant darkness (**Supplementary Fig. 4b**), indicating that the lifespan shortening effects of light exposure are primarily mitigated by the photoreceptors.

We performed survival analyses in rhodopsin null flies to examine how activation of the different photoreceptor subtypes influence lifespan on AL and DR. In agreement with the reduction in systemic immune responses observed in the rhodopsin null strains,

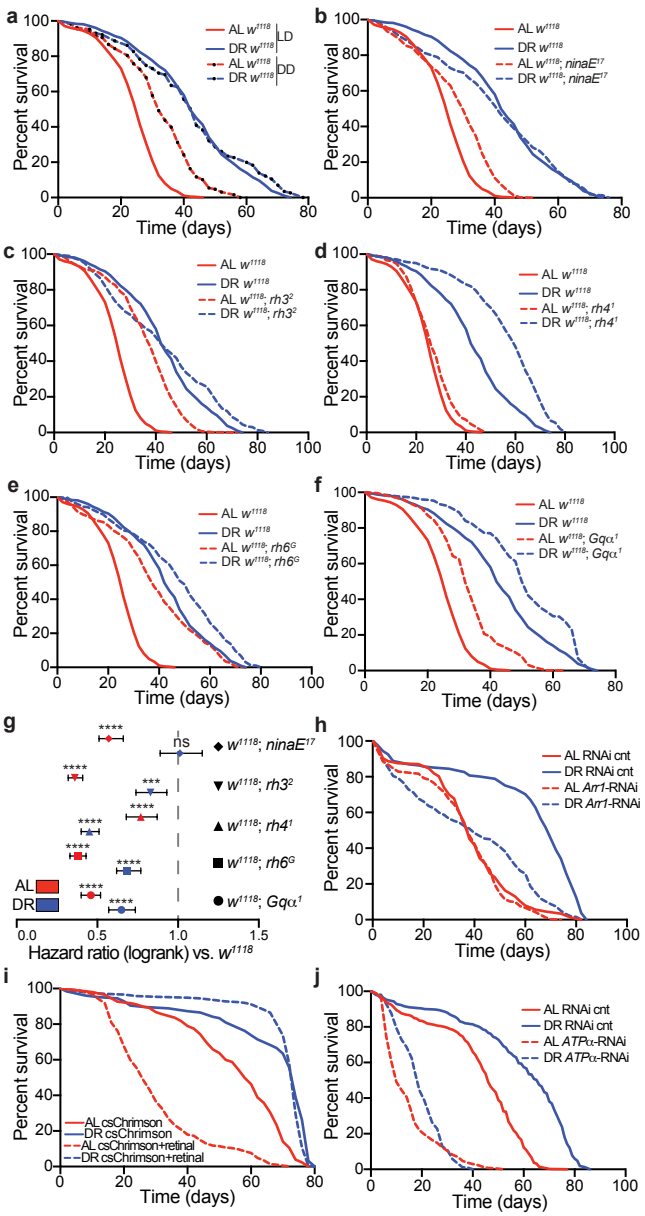

Figure 4. Photoreceptor activation modulates lifespan in a diet-dependent fashion. (**a**) Survival analysis of w^{1118} flies housed in 12:12h LD or constant darkness (DD). Survival data is plotted as an average of three independent lifespan repeats. LD housed flies: AL *N*=560, DR *N*=584; DD: AL *N*=460, DR *N*=462. (**b-f**) Survival analysis of w^{1118}; $ninaE^{17}$, w^{1118}; $rh3^2$, w^{1118}; $rh4^1$, w^{1118}; $rh6^G$, and w^{1118}; $Gq\alpha^1$ mutants compared to w^{1118} control flies housed in 12:12h LD. Survival data is plotted as an average of three independent lifespan repeats. *Survival curves for w^{1118} are re-plotted (b-f) for visual comparison, and the w^{1118} and rhodopsin null lifespans repeats were performed simultaneously. All mutant lines were outcrossed to w^{1118}. w^{1118}; $ninaE^{17}$ flies: AL *N*=514, DR *N*=511; w^{1118}; $rh3^2$ flies: AL *N*=543, DR *N*=597; w^{1118}; $rh4^1$ flies: AL *N*=550, DR *N*=593; w^{1118}; $rh6^G$ flies: AL *N*=533, DR *N*=563; w^{1118}; $Gq\alpha^1$ flies: AL *N*=403, DR *N*=400. (**g**) Hazard ratios for rhodopsin and Gq mutant flies compared to w^{1118} control flies (ratios<1 indicate flies that are more likely to survive compared to w^{1118}). Error bars indicate the 95% confidence interval of the hazard ratios. (**h**) Survival analysis of eye-specific *arr1*-RNAi knockdown flies vs RNAi control flies. Survival data is plotted as an average of two independent lifespan repeats for *arr1*-RNAi and one independent lifespan replicate for RNAi-controls. RNAi control flies: AL *N*=177, DR *N*=161; *arr1*-RNAi flies: AL *N*=333, DR *N*=322. (**i**) Survival analysis of retinal inducible, photoreceptor-specific optogenetic flies (Trpl-GAL4>UAS-csChrimson[red-shifted]) supplemented with retinal or vehicle control and housed in 12:12h red-light:dark. Survival data is plotted as an average of two independent lifespan repeats. Retinal treated flies: AL *N*=289, DR *N*=236; Vehicle treated flies: AL *N*= 256, DR *N*=126. (**j**) Survival analysis of eye-specific *ATPα* RNAi knockdown flies vs RNAi control flies. Survival data is plotted as an average of three independent lifespan repeats. RNAi control flies: AL *N*=493, DR *N*= 490; *ATPα* RNAi flies: AL *N*=510, DR *N*=535. (g) *P*values were determined by Log-rank (Mantel-Cox) test, ns denotes a non-significant *p*values, **** indicates *p*values less than 0.0001.

these flies were also longer lived in comparison to w^{1118} outcrossed controls (**Fig. 4b-e**). Furthermore, $rh6^{G}$ mutants, which displayed the largest reductions in inflammation, also displayed the greatest extension in lifespan compared to the other rhodopsin null lines. $Gq\alpha^{1}$ mutants [43], which harbor a mutation in the G-protein that mediates activation of TRP channels downstream of rhodopsin, also displayed increased longevity compared to control flies (**Fig. 4f**). Interestingly, with the exception of Rh4, rhodopsin null mutations and $Gq\alpha^{1}$ mutants primarily extended lifespan on AL, indicated by the hazard ratios in **Fig. 4g**. We next sought to investigate how increases in rhodopsin-mediated signaling influence survival. To this end, we knocked down the major arrestin protein, *arr1*, within the eyes of flies (GMR-GAL4>UAS-*arr1*-RNAi). Arr1 is required for light-mediated rhodopsin internalization from the rhabdomere membrane into endocytic vesicles, thus suppressing rhodopsin-mediated signaling and associated Ca^{2+}-mediated phototoxicity/cell death [19, 44, 45]. In agreement with its physiological role in light-adaptation, we found that *arr1*-RNAi knockdown flies were hypersensitized to light (**Supplementary Fig. 4i**). In contrast to the Rhodopsin null strains which displayed greater proportional improvements in survival on AL vs DR, *arr1*-RNAi knockdown flies displayed significantly lifespan shortening on DR, while the lifespan on AL was indistinguishable from the control (**Fig. 4h**). Together, these data argue that DR-protects against lifespan shortening downstream of light and/or rhodopsin-mediated signaling in a manner that requires light-adaptation, and by extension, *arr1*-mediated rhodopsin endocytosis.

We utilized an optogenetics approach to examine how chronic photoreceptor activation influences survival in flies reared on AL or DR. Optogenetics is a powerful tool for examining how photoreceptor activation/suppression influences lifespan as it allows for the ability to compare lifespans within flies reared under the same lighting conditions, thus diminishing potential confounding variables present when comparing lifespan in different lighting conditions (i.e., LD vs constant darkness), such as extra-ocular effects of light on survival. To generate optogenetic flies we expressed the red-light-sensitive csChrimson cation channel [46] within photoreceptors (Trpl-GAL4>UAS-csChrimson). To activate the csChrimson channels, we housed the optogenetic flies in a 12:12 red-light:dark cycle and supplemented their food with either all-*trans* retinal (a chromophore required for full activation of csChrimson channels [47]) or a vehicle control (**Supplementary Fig. 4c**). Optogenetic activation of the photoreceptors (retinal treated) drastically reduced AL lifespan compared to vehicle treated controls, while the lifespan on DR was unaffected (**Fig. 4i**). Retinal did not appear to be toxic to flies lacking csChrimson channels, as the lifespan of *Canton-S* wild-type flies were indistinguishable between vehicle and retinal treated groups (**Supplementary Fig. 4d**).

Although DR protected flies from lifespan shortening from the optogenetic activation of photoreceptors, we found that forcing photoreceptor degeneration, by knocking down *ATPα* in the eye shortened lifespan on both AL and DR (**Fig. 4j**). Similarly, eye-specific knockdown of *nervana-2* and *-3* (*nrv2,* GMR-GAL4>UAS-*nrv2*-RNAi and *nrv3*,

317 GMR-GAL4>UAS-*nrv3*-RNAi), which encode the *Beta* subunit of the Na^+K^+ATPase of the
318 eye [31] also reduced phototaxis responses and shortened lifespan (**Supplementary Fig.**
319 **4e-h**). Taken together, these data support a model where DR protects flies from lifespan
320 shortening caused by photoreceptor stress, as chronic photoreceptor activation reduces
321 survival in flies reared on AL while having minimal to no effect on flies reared on DR.
322 Inversely, photoreceptor deactivation primarily improves survival of flies reared on AL.

323 *Eye-specific, CLK-output genes modulate lifespan*

324 We next sought to determine if CLK-output genes in the eye influence age-related visual
325 declines and lifespan. We employed a bioinformatics approach to identify candidate eye-
326 specific circadian genes transcriptionally regulated by CLK (**Supplementary Fig. 5a and**
327 **Supplemental Data 6**). First, we compared age-associated changes in photoreceptor-
328 enriched gene expression [5] to genes that were differentially expressed on DR compared
329 to AL. More than half of the photoreceptor-enriched genes that were downregulated with
330 age were also upregulated on DR at ZT 0 and ZT 12 (**upper left quadrant of Fig. 5a, b and**
331 **Supplementary Fig. 5a**). We then subset this gene list, selecting just transcripts whose
332 expression was downregulated with age and upregulated on DR, and examined how their
333 expression changed in nCLK-Δ1 fly heads (**Supplementary Fig. 5a**). From this analysis, we
334 identified *Gβ76c*, *retinin,* and *sunglasses* as genes that were significantly downregulated
335 in nCLK-Δ1 fly heads at ZT 0 and/or ZT 12 (**Fig. 5c, d and Supplementary Fig. 5a, e-g**).
336 *Gβ76c* encodes the eye-specific G beta subunit that plays an essential role in terminating

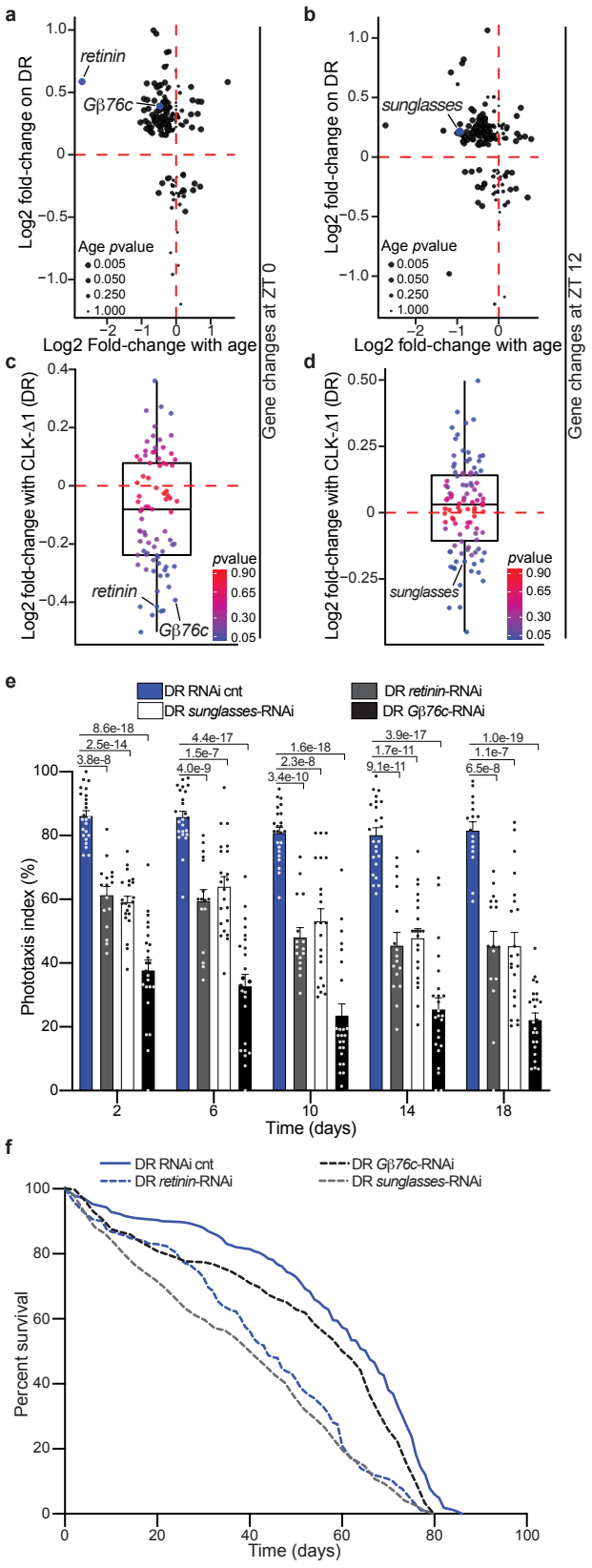

Figure 5. Knockdown of DR-sensitive, eye-specific CLK-output genes reduces survival. (**a-b**) Scatterplot of circadian, photoreceptor-enriched gene changes with age in wild-type heads (*x*-axis: 5- *vs* 55-day old flies) *vs* diet-dependent gene expression changes in heads from nCLK-Δ1 RNA-Seq control flies (*y*-axis: DR- *vs* AL-minus RU486) at ZT 0 (a) and ZT 12 (b). (**c-d**) Boxplots of the expression changes in nCLK-Δ1 heads (DR plus- *vs* DR minus-RU486) at ZT 0 (c) and ZT 12 (d) of genes that were downregulated with age and upregulated on DR (upper left quadrants of Fig. 5a, b). (**e**) Positive phototaxis responses with eye-specific knockdown of *Gβ76c* (GMR-GAL4> UAS-*Gβ76c*-RNAi), *retinin* (GMR-GAL4>UAS-*retinin*-RNAi), and *sunglasses* (GMR-GAL4>UAS-*sunglasses*-RNAi) compared to RNAi control flies (GMR-GAL4>UAS-*mCherry*-RNAi) reared on DR. For each timepoint results are represented as average phototaxis response +/-SEM (RNAi control *n*=24 biological replicates, *N*=480 flies per condition; *Gβ76c* RNAi *n*=24 biological replicates, *N*=480 flies per condition; *retinin* RNAi *n*=16 biological replicates, *N*=384 flies per condition; *sunglasses* RNAi *n*=24 biological replicates, *N*=480 flies per condition). (**f**) Survival analysis of eye-specific *Gβ76c*, *retinin*, *sunglasses*, and RNAi knockdown flies compared to RNAi control flies reared on DR. Survival data is plotted as an average of three independent lifespan repeats for RNAi control, *sunglasses*, and *Gβ76c* flies and two independent lifespan repeats for *retinin* RNAi knockdown flies. RNAi-cnt flies: *N*=490; *retinin*-RNAi flies: *N*=363; *sunglasses*-RNAi flies: *N*=468; *Gβ76c*-RNAi flies: *N*=509. (e) *P*values were determined by two-tailed Student's ttest (unpaired) at each timepoint comparing the phototaxis index of RNAi control flies to *Gβ76c*-, *retinin*-, and *sunglasses*-RNAi flies.

phototransduction [13, 48]. *Retinin* encodes one of the four most highly expressed proteins in the lens of the *Drosophila* compound eye [49]. Furthermore, *retinin* functions in the formation of corneal nanocoatings, knockdown of which results in degraded nanostructures and a reduction in their anti-reflective properties [50]. *Sunglasses*, also called *Tsp42Ej*, encodes for a lysosomal tetraspanin concentrated in the retina that protects against photoreceptor degeneration by degrading rhodopsin in response to light [51]. We analyzed a published CLK Chromatin Immunoprecipitation (ChIP-chip) dataset in flies and observed rhythmic CLK binding at the 5'-untranslated region of *sunglasses* in *Drosophila* eye tissue [52] (**Supplementary Fig. 5h and Supplementary Table 1**), which supports our bioinformatics approach and provides further evidence that *sunglasses* is an eye-specific CLK-output gene. Eye-specific knockdown of *Gβ76c* (GMR-GAL4>UAS-*Gβ76c*-RNAi), *retinin* (GMR-GAL4>UAS-*retinin*-RNAi), and *sunglasses* (GMR-GAL4>UAS-*sunglasses*-RNAi) reduced phototaxis responses (**Fig. 5e and Supplementary Fig. 5i**), and shortened lifespan in comparison to RNAi control flies (GMR-GAL4>UAS-*mCherry*-RNAi) (**Fig. 5f, Supplementary Fig. 5j**). These findings indicate that DR and CLK function together in the regulation of eye-specific circadian genes involved in the negative regulation of rhodopsin signaling (i.e., phototransduction termination). Furthermore, these observations support previous findings that lifespan extension upon DR requires functional circadian clocks [10, 53], and establishes CLK-output genes as diet-dependent regulators of eye aging and lifespan in *Drosophila*.

Discussion

Progressive declines in circadian rhythms are one of the most common hallmarks of aging observed across most lifeforms [54]. Quantifying the strength, or amplitude, of circadian rhythms is an accurate metric for predicting chronological age [55]. Many cellular processes involved in aging (e.g., metabolism, cellular proliferation, DNA repair mechanisms, etc.) display robust cyclic activities. Both genetic and environmental disruptions to circadian rhythms are associated with accelerated aging and reduced longevity [56, 57]. These observations suggest that circadian rhythms may not merely be a biomarker of aging; rather, declines in circadian rhythms might play a causal role. The observation that DR and DR-memetics, such as calorie restriction and time-restricted feeding, improve biological rhythms suggests that clocks may play a fundamental role in mediating their lifespan-extending benefits.

Herein, we identified circadian processes that are selectively amplified by DR. Our findings demonstrate that DR amplifies circadian homeostatic processes in the eye, some of which are required for DR to delay visual senescence and improve longevity in *Drosophila*. Taken together, our data demonstrate that photoreceptor stress has deleterious effects on organismal health; disrupting CLK function and/or overstimulation of the photoreceptors induced a systemic immune response and reduced longevity. Our findings establish the eye as a diet-sensitive regulator of lifespan. DR's neuroprotective role in the photoreceptors appears to be mediated via the molecular clock, which promotes the

377 rhythmic oscillation of genes involved in the suppression of phototoxic cell stress (**Fig. 6**
378 **and Supplemental Discussion 1**). Our data also support the idea that age-related declines
379 in the visual system impose a high cost on an organism. Perhaps this is why a number of
380 long-lived animals have visual systems that have undergone regressive evolution (e.g.,
381 cave-dwelling fish and naked-mole rats) [58]. Failing to develop a visual system may help
382 these organisms avoid age-related damage and inflammation caused by retinal
383 degeneration. Ultimately, developing a visual system, which is critical for reproduction
384 and survival, may be detrimental to an organism later in life. Thus, vision may be an
385 example of an antagonistically pleiotropic mechanism that shapes lifespan.
386

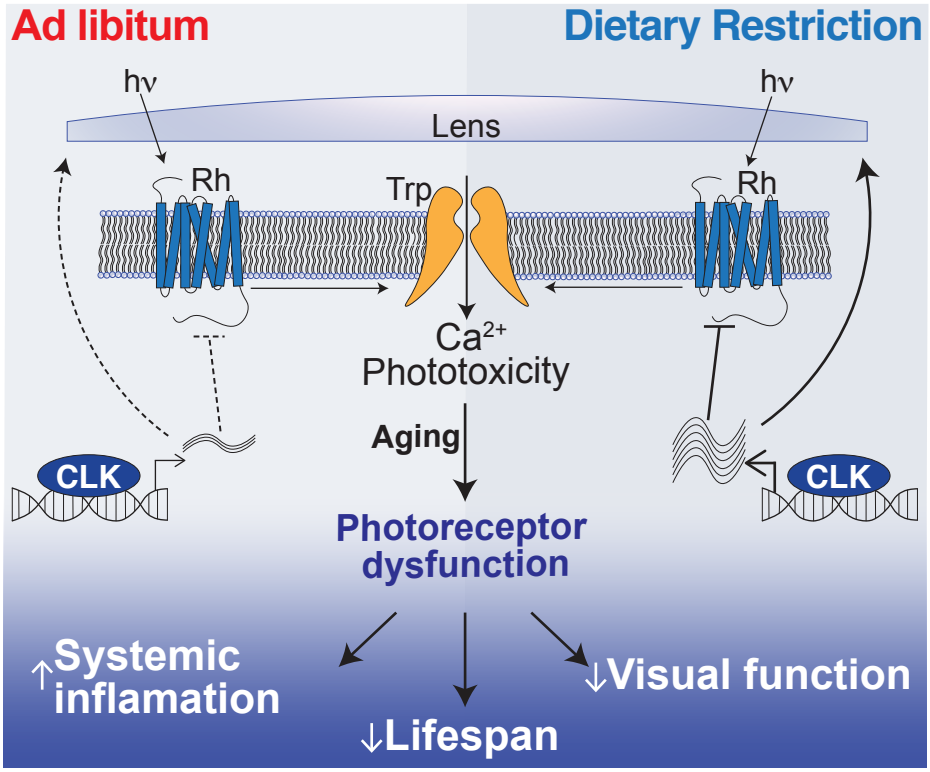

Fig. 6. Dietary restriction extends lifespan by promoting rhythmic homeostatic processes in the eye. DR promotes CLK-output processes in the eye that suppress light/Ca^{2+}-mediated phototoxicity to suppress systemic inflammaion, delay visual senesence, and improve survival.

Methods

Fly stocks: The genotypes of the *Drosophila* lines used in this study are listed in **Supplemental Table 2**. The following lines were obtained from the Bloomington *Drosophila* Stock Center: *Oregon R.* (25125), GMR-GAL4 (1104), Elav-GS-GAL4 (43642), Trpl-GAL4 (52274), Clk^{OUT} (56754), UAS-csChrimson (55134), UAS-CLK-Δ1 (36318), UAS-CLK-Δ2 (36319), *Gβ76c*-RNAi (28507), *tsp42Ej/sunglasses*-RNAi (29392), *retinin*-RNAi (57389), *ATPα*-RNAi (28073), *nrv2*-RNAi (28666), *nrv3*-RNAi (60367), and mCherry-RNAi (Bloomington RNAi-cnt, 35785). The following lines were obtained from the Vienna *Drosophila* Resource Center: *arr1*-RNAi (22196), *RNAi*-cnt (empty vector, 60100). The following lines were received from the laboratory of Craig Montell: *CantonS*, w^{1118}, w^{1118}; $ninaE^{17}$, w^{1118}; $rh3^{2}$, w^{1118}; $rh4^{1}$, w^{1118}; $rh6^{G}$, w^{1118}; $Gq\alpha^{1}$, and TRP^{365}. The following lines were outcrossed to w^{1118} for this manuscript: UAS-CLK-$\Delta1^{OC}$ and $CantonS^{OC}$. The Trpl-GAL4 line was recombined with GAL80 for this manuscript: Trpl-GAL4; $GAL80^{ts}$.

Fly husbandry and survival analyses: All flies were maintained at 25±1 °C, 60% humidity under a 12h:12h LD cycle (~750lux, as measured with a Digital Lux Meter, Dr. Meter Model LX1330B) unless otherwise indicated. Fly stocks and crosses were maintained on a standard fly media as described previously [59]. Briefly, standard fly media consisted of 1.5% yeast extract, 5% sucrose, 0.46% agar, 8.5% of corn meal, and 1% acid mix (a 1:1 mix of 10% propionic acid and 83.6% phosphoric acid). Fly bottles were seeded with live yeast

prior to collecting virgins or setting up crosses. Mated adult progeny were then transferred to *ad libitum* (AL) or dietary restriction (DR) media within three days of eclosion. Adult flies used in experiments were transferred to fresh media every 48h at which point deaths were recorded for survival analysis. AL and DR fly media differed only in its percentage of yeast extract, respectively containing 5% or 0.5% (Yeast Extract, B.D. Bacto, Thermo Scientific 212720, Cat no. 90000-722). *Optogenetic experiments*: For experiments using the csChrimson channel rhodopsin [46], adult flies were transferred to media supplemented with 50µM all-trans-retinal (Sigma Aldrich, R2500-1G) or drug vehicle (100% ethanol), and maintained under a 12h:12h red light:dark cycle, with ~10lux of red light (~590nm) during the light phase. *Elav-GeneSwitch flies*: GeneSwitch [60], adult flies were transferred to media supplemented with 200µM RU486 (Mifepristone, United States Biological), indicated as either AL+ or DR+, for post-developmental induction of transgenic elements; isogenic control flies were transferred to food supplemented with a corresponding concentration of drug vehicle (100% ethanol), indicated as either AL- or DR-. *prCLK-Δ1 experiments*: GAL80 temperature sensitive crosses were set in bottles at 25°C, 60% humidity under a 12h:12h LD cycle for four days. Parental flies were removed, and the bottles were transferred to 18°C for approximately three-weeks to suppress GAL4 activity throughout development. After ecolsion, the F1 generations were sorted onto AL or DR food the flies were maintained at 30°C to de-repress GAL80 and activate GAL4 (60% humidity under a 12h:12h LD cycle) for the remainder of their lifespans. The F1

generations for these experiments share the same genetic background, as both the UAS-CLK-Δ1 and the *CantonS* control lines were fully outcrossed to the same w^{1118} strain prior to setting up the cross with Trpl-GAL4; $GAL80^{ts}$.

Circadian time-course expression analysis: Mated *Canton-S* females were reared on AL or DR diets for seven days at 25±1 °C, under a 12:12h light-dark (LD) regimen. Beginning on the seventh day, four independent biological replicates (per diet/timepoint) of approximately 35 flies were collected on dry ice every four-hours for 20-hours starting at ZT 0 (six total timepoints, 48 total samples). RNA extraction, DNA amplification/labeling, and gene expression arrays were performed following the same protocols as in Katewa *et al.*, 2012 [61]. In summary, RNA was isolated from whole fly lysates with Qiagen's RNeasey Lipid Tissue Mini Kit (74804) and RNA quantity and quality were accessed with a Nanodrop and Agilent's bioanalyzer (RNA 600 Nano Kit (5067-15811)). DNA amplification from total RNA was performed using Sigma's TransPlex Complete Whole Transcriptome Amplification Kit (WTA2) and purified with Qiagen's QIAquick PCR Purification Kit (28104). Gene expression labeling was performed with NimbleGen One-Color DNA Labeling Kit (05223555001) and hybridized to NimbleGen 12-Plex gene expression arrays. Arrays were quantitated with NimbleGen's NimbleScan2 software, and downstream expression analyses were conducted in R (http://www.r-project.org). Transcript-level expression from the four independent biological replicates were averaged for each time-point.

nCLK-Δ1 RNA-Seq analyses: nCLK-Δ1 (Elav-GS-GAL4>UAS-nCLK-Δ1) adult flies were developed on standard stock food (1.5% yeast-extract) for four days. Three independent biological replicates of 100 mated female flies were then reared on AL or DR diets treated with RU486 or vehicle control at 25±1 °C, under a 12:12h LD regimen. Diets were changed approximately every 48-hours, until the seventh day at which point flies were flash frozen on dry-ice at ZT 0 and ZT 12 (lights-on and -off, respectively). See Supplemental Fig. 2a for RNA-Seq. experimental design. *RNA-extraction*: Frozen flies were vortexed to remove heads and mRNA from each biological replicate of pooled heads was isolated with the Quick-RNA MiniPrep Kit (Zymo Research #11-328), per manufactures' instructions. *Fragment library preparation and deep sequencing*: Library preparation was performed by the Functional Genomics Laboratory (FGL), a QB3-Berkeley Core Research Facility at University of California, Berkeley. cDNA libraries were produced from the low-input RNA using the Takara SMART-Seq v4 Ultra-low input RNA kit. An S220 Focused-Ultrasonicator (Covaris®) was used to fragment the DNA, and library preparation was performed using the KAPA hyper prep kit for DNA (KK8504). Truncated universal stub adapters were used for ligation, and indexed primers were used during PCR amplification to complete the adapters and to enrich the libraries for adapter-ligated fragments. Samples were checked for quality on an AATI (now Agilent) Fragment Analyzer. Samples were then transferred to the Vincent J. Coates Genomics Sequencing Laboratory (GSL), another QB3-Berkeley

Core Research Facility at UC Berkeley, where Illumina sequencing library molarity was measured with quantitative PCR with the Kapa Biosystems Illumina Quant qPCR Kits on a BioRad CFX Connect thermal cycler. Libraries were then pooled evenly by molarity and sequenced on an Illumina NovaSeq6000 150PE S4 flowcell, generating 25M read pairs per sample. Raw sequencing data was converted into fastq format, sample specific files using the Illumina bcl2fastq2 software on the sequencing centers local linux server system. *Read alignment and differential expression analyses*: Raw fastq reads were filtered by the Trimmomatic software [62] (Trimmomatic-0.36) to remove Illumina-specific adapter sequences and the minimal length was set to 36 (MINLEN) for trimming sequences. The paired end filtered reads were then aligned to the *D. Melanogaster* dm6 genome (BDGP Release 6 + ISO1 MT/dm6) by HISAT2 [63] to generate BAM files with the specific strand information set to "Reverse". Count files were then generated by featureCounts [64] and the *D. Melanogaster* reference genome was utilized as the gene annotation file with specific strand information set to "stranded (Reverse)". Resulting count files (tabular format) were then analyzed with DEseq2 [65] with fit-type set to "local", and *p*values of less than 0.05 were considered differentially expressed between factor levels. Normalized count reads were outputted for visualization of expression (heatmaps), and Supplemental Data Files 3a contains normalized count reads across all experimental samples. *UCSC genome browser visualization*: The makeUCSCfile software package from HOMER was

utilized to generate bedGraph files for visualizing changes in tag density at exon 2 of *clk* comparing nCLK-Δ1 and control samples (Supplementary Fig. 2B).

Heatmap visualizations: We employed the heatmap2 function from R gplots package to visualize bioinformatics data. Data were not clustered, and data were scaled by row for normalization across time-points.

Electroretinogram assays: ERGs were performed and analyzed in two independent laboratories. ERGs were recorded for nCLK-Δ1 flies reared on AL or DR diets supplemented with vehicle or RU486 at day 14 at the Baylor College of Medicine (BCM), and at day 21 at the University of California, Santa Barbara (UCSB). ERGs were recorded for prCLK-Δ1 flies at UCSB reared on AL or DR and maintained at either 18°C or 30°C. *BCM*: ERG recordings were performed as in Wang *et al.*, 2014 [66]. Flies were glued on a glass slide. A recording electrode was placed on the eye and a reference electrode was inserted into the back of the fly head. Electrodes were filled with 0.1 M NaCl. During the recording, a 1 s pulse of light stimulation was given. The ERG traces of at least eight flies per genotype/diet were recorded and analyzed by LabChart8 software (AD Instruments). *UCSB*: ERG recordings were performed as in Wes *et al.*, 1999 [67]. Two glass electrodes were filled with Ringer's solution and electrode cream was applied to immobilized flies. A reference electrode was placed on the thorax, while the recording electrode was placed

506 on the eyes. Flies were then exposed to a 10s pulse of ~200lux white light, a light intensity
507 that is comparable to the phototaxis assay. An EI-210 amplifier (Warner Instruments) was
508 used for amplifying the electrical signal from the eye after light stimulation, and the data
509 were recorded using a Powerlab 4/30 device along with the LabChart 6 software (AD
510 Instruments). Raw data were then uploaded into R-statistical software for plotting and
511 statistical analysis. All electroretinograms were performed between ZT4-8 or ZT12-14.
512
513 Positive phototaxis assay: Positive phototaxis was performed using an adapted protocol
514 from Vang *et al.*, 2014 [68] (Fig S2D). Phototaxis measurements were recorded
515 longitudinally on populations of female flies aged on either AL or DR food (with or without
516 200μM RU486 when indicated) at a density of 10-25 flies per tube prior to and after
517 phototaxis measurements. On the day of phototaxis recording, eight groups of flies (four
518 AL and four DR groups) were placed in separate 2.5cm x 20cm tubes (created from three
519 enjoined narrow fly vials [Genesee Scientific]) and dark-adapted for 15-minutes prior to
520 light exposure (no food was available in the vials during phototaxis assays). Flies were
521 then gently tapped to the bottom of the tube, placed horizontally, and exposed to white
522 light from an LED strip (Ustellar, UT33301-DW-NF). A gradient of light intensity was
523 created, with 500lux at the nearest point in the fly tube to the light source and 150lux at
524 the furthest point. Phototaxis activity was recorded by video at 4K resolution (GoPro,
525 Hero5 black). Positive phototaxis was scored manually as the percentage of flies that had

traveled >19cm toward the light source in three 15s intervals (15s, 30s, and 45s). "Phototaxis index" was calculated by averaging the percent of positive phototaxis for each vial at the three 15s intervals. To control for light-independent wandering activity, a phototaxis index was also calculated when the light source was placed in parallel to the fly tube, such that all parts of the tube were equally illuminated with 500lux. *Normalizing phototaxis responses to wandering activity failed to significantly affect phototaxis index, data not shown.

RNA extraction and cDNA preparation: Flies were maintained on AL or DR for the indicated amount of time, then flash frozen on dry ice. Heads were separated from bodies (thorax and abdomen) by vigorous shaking. Flies were then ground using a hand-held homogenizer at room temperature following MiniPrep instructions. Total RNA was isolated using the Quick-RNA MiniPrep Kit (Zymo Research, 11-328). In brief, flies were maintained on AL or DR for the indicated amount of time, then flash frozen on dry ice. Heads were separated from bodies (thorax and abdomen) by vigorous shaking. Flies were then ground using a hand-held homogenizer at room temperature following MiniPrep instructions. RNA was collected into 30µl DNAse/RNAse-free water and quantified using the NanoDrop 1000 Spectrophotometer (Thermo Scientific). For each experiment, 120-180 age-, genotype-, and diet-matched flies were collected, and three independent RNA extractions were performed. To extract RNA from heads, 40-60 flies were used; to extract

546 RNA from bodies, 20-30 flies were used. *cDNA preparation*: The iScript Reverse
547 Transcription Supermix for RT-qPCR (Bio-Rad, 1708841) was used to generate cDNA from
548 RNA extracted from heads and bodies. For each group, 1 µg of total RNA was placed in a
549 volume of 4µl iScript master mix, then brought to 20µl with DNAse/RNAse-free water. A
550 T1000 thermocycler (BioRad) was used for first-strand RT-PCR reaction following iScript
551 manufacturers' instructions—priming step (5min at 25°C), reverse transcription (30min at
552 42°C), and inactivation of the reaction (5min at 85°C).
553 Real-time quantitative PCR: Reactions were performed in a 384-well plate. Each reaction
554 contained 2µl of 1:20 diluted cDNA, 1µl of primers (forward and reverse at 10µM), 5µl
555 SensiFAST SYBR Green No-ROX Kit (BIOLINE, BIO-98020), and 2µl of DNAse/RNAse-free
556 water. The qPCR reactions were performed with a Light Cycler 480 Real-Time PCR machine
557 (Roche Applied Science) with the following run protocol: pre-incubation (95°C for 2 min),
558 forty PCR cycles of denaturing (95°C for 5s, ramp rate 4.8°C/s), and annealing and
559 extension (60°C for 20 s, ramp rate 2.5°C/s).
560
561 Hemolymph Mass spectrometry: *Proteomic sample preparation*: nCLK-Δ1 female flies
562 (Elav-GeneSwitch-GAL4>UAS-nCLK-Δ1) were reared on AL diet plus RU486 or vehicle
563 control (*N*=300 flies per biological replicate, *n*=3 biological replicates). At day 14, flies
564 were snap frozen on dry ice and transferred to pre-chilled vials. The vials were vortexed
565 for 5-10s to remove heads and the frozen bodies were transferred to room temperature

566 vials fitted with 40µm filters. Headless bodies were thawed at room temperature for 5
567 minutes and spun at 5000 rpm for 10min at 4 °C. Following the spin, hemolymph collected
568 at the bottom of each vial and the bodies remained within the filters. *Digestion*: A
569 Bicinchoninic Acid protein assay (BCA) was performed for each of the hemolymph samples
570 and a 100µg aliquot was used for tryptic digestion for each of the 6 samples. Protein
571 samples were added to a lysis buffer containing a final concentration of 5% SDS and 50
572 mM triethylammonium bicarbonate (TEAB), pH ~7.55. The samples were reduced in 20
573 mM dithiothreitol (DTT) for 10 minutes at 50º C, subsequently cooled at room temperature
574 for 10 minutes, and then alkylated with 40 mM iodoacetamide (IAA) for 30 minutes at
575 room temperature in the dark. Samples were acidified with a final concentration of 1.2%
576 phosphoric acid, resulting in a visible protein colloid. 90% methanol in 100 mM TEAB was
577 added at a volume of 7 times the acidified lysate volume. Samples were vortexed until the
578 protein colloid was thoroughly dissolved in the 90% methanol. The entire volume of the
579 samples was spun through the micro S-Trap columns (Protifi) in a flow-through Eppendorf
580 tube. Samples were spun through in 200 µL aliquots for 20 seconds at 4,000 x g.
581 Subsequently, the S-Trap columns were washed with 200 µL of 90% methanol in 100 mM
582 TEAB (pH ~7.1) twice for 20 seconds each at 4,000 x g. S-Trap columns were placed in a
583 clean elution tube and incubated for 1 hour at 47º C with 125 µL of trypsin digestion buffer
584 (50 mM TEAB, pH ~8) at a 1:25 ratio (protease:protein, wt:wt). The same mixture of trypsin
585 digestion buffer was added again for an overnight incubation at 37º C.

586 Peptides were eluted from the S-Trap column the following morning in the same elution
587 tube as follows: 80 µL of 50 mM TEAB was spun through for 1 minute at 1,000 x g. 80 µL
588 of 0.5% formic acid was spun through next for 1 minute at 1,000 x g. Finally, 80 µL of 50%
589 acetonitrile in 0.5% formic acid was spun through the S-Trap column for 1 minute at 4,000
590 x g. These pooled elution solutions were dried in a speed vac and then re-suspended in
591 0.2% formic acid. *Desalting*: The re-suspended peptide samples were desalted with stage
592 tips containing a C18 disk, concentrated and re-suspended in aqueous 0.2% formic acid
593 containing "Hyper Reaction Monitoring" indexed retention time peptide standards (iRT,
594 Biognosys). *Mass spectrometry system*: Briefly, samples were analyzed by reverse-phase
595 HPLC-ESI-MS/MS using an Eksigent Ultra Plus nano-LC 2D HPLC system (Dublin, CA) with
596 a cHiPLC system (Eksigent) which was directly connected to a quadrupole time-of-flight
597 (QqTOF) TripleTOF 6600 mass spectrometer (SCIEX, Concord, CAN). After injection,
598 peptide mixtures were loaded onto a C18 pre-column chip (200 µm x 0.4 mm ChromXP
599 C18-CL chip, 3 µm, 120 Å, SCIEX) and washed at 2 µl/min for 10 min with the loading
600 solvent (H_2O/0.1% formic acid) for desalting. Subsequently, peptides were transferred to
601 the 75 µm x 15 cm ChromXP C18-CL chip, 3 µm, 120 Å, (SCIEX), and eluted at a flow rate
602 of 300 nL/min with a 3 h gradient using aqueous and acetonitrile solvent buffers. *Data-*
603 *dependent acquisitions (for spectral library building)*: For peptide and protein
604 identifications the mass spectrometer was operated in data-dependent acquisition [51]
605 mode, where the 30 most abundant precursor ions from the survey MS1 scan (250 msec)

were isolated at 1 m/z resolution for collision induced dissociation tandem mass spectrometry (CID-MS/MS, 100 msec per MS/MS, 'high sensitivity' product ion scan mode) using the Analyst 1.7 (build 96) software with a total cycle time of 3.3 sec as previously described [69]. *Data-independent acquisitions*: For quantification, all peptide samples were analyzed by data-independent acquisition (DIA, e.g. SWATH), using 64 variable-width isolation windows [70, 71]. The variable window width is adjusted according to the complexity of the typical MS1 ion current observed within a certain m/z range using a DIA 'variable window method' algorithm (more narrow windows were chosen in 'busy' m/z ranges, wide windows in m/z ranges with few eluting precursor ions). DIA acquisitions produce complex MS/MS spectra, which are a composite of all the analytes within each selected Q1 m/z window. The DIA cycle time of 3.2 sec included a 250 msec precursor ion scan followed by 45 msec accumulation time for each of the 64 variable SWATH segments.

Identification of photoreceptor enriched CLK-output genes: Diagram of bioinformatics steps reported in Supplementary Fig. 5A. Gene-lists are reported in **Supplemental Data 6**. We identified the top 1,000 photoreceptor-enriched genes from Charlton-Perkins *et al.*, 2017 [72] (GSE93782). We then filtered this list for genes that oscillate in a circadian fashion, and that are downregulated with age from Kuintzle *et al.*, 2017 [15] (GSE81100). Approximately 1/3 of the photoreceptor enriched genes (366 genes) were expressed in a

626 circadian fashion in young wild-type heads and approximately one-half of these (172
627 genes) displayed a significant loss in expression with age (5- vs 55-day old heads). We
628 further analyzed the remaining gene lists to identify those that are significantly
629 upregulated on DR compared to AL at either ZT 0 or ZT 12 from control (vehicle treated)
630 samples from our nCLK-Δ1 RNA-Seq analyses. For the final filtering step, we analyzed the
631 genes that were significantly downregulated in nCLK-Δ1 on DR (RU486 vs vehicle treated
632 controls), resulting in the identification of *Gβ76c*, *retinin*, and *sunglasses*.
633
634 **Statistical analysis**
635 The individual biological replicates "*n*" and the number of individual flies "*N*" is denoted
636 in each figure legend along with the particular statistical test utilized. The *p*value statistics
637 are included in each figure. All error bars are represented as standard error of the mean
638 (SEM), and all graphs were generated in PRISM 9 (GraphPad). The experiments in this
639 manuscript were performed with populations of female flies (i.e., typically greater than 20
640 flies per technical replicate).
641 Time-course microarray analyses: Four independent biological replicates (per
642 diet/timepoint) of approximately 35 *CantonS* female flies were collected on dry ice every
643 four-hours for 20-hours starting at ZT 0 (six total timepoints, 48 total samples). Differential
644 expression was determined by two-tailed Student's *t*test (paired) comparing the averaged
645 transcript-level expression values between AL and DR samples across all timepoints, and

646 *p*values less than 0.05 were considered significant. The JTK_CYCLE algorithm [73] (v3.0)
647 was utilized to identify circadian transcripts from the AL and DR time-course expression
648 arrays. Transcript level expression values for each of the four biological replicates (per
649 timepoint/diet) were used as input for JTK_CYCLE, and period length was set to 24-hours.
650 We defined circadian transcripts as those displaying a JTK_CYCLE *p*value of less than 0.05.
651 Subsequent analyses compared diet-dependent changes in JTK_CYCLE outputs (phase
652 and amplitude).
653 nCLK-Δ1 RNA-Seq: Three independent biological replicates of 100 mated female adult
654 flies were utilized per genotype/diet/time-point. DEseq2 software [65] was utilized and
655 *p*values of less than 0.05 were considered differentially expressed between factor levels.
656 ERG responses: For ERG experiments we quantified responses from 6-15 individual flies
657 per standards in the field. Statistical significance was determined by two-tailed Student's
658 *t*test (unpaired), comparing ERG responses between diet and genotypes. Full ERG statistics
659 are reported in **Supplemental Data 10**.
660 Survival analyses: The Log-rank (Mantel-Cox) test was used to determine statistical
661 significance comparing average lifespan curves from a minimum of two independent
662 lifespan replicates. Hazard Ratios (logrank) were also utilized to determine the probability
663 of death across genotypes, lighting conditions, and diet. Detailed Log-rank and hazard
664 ratios for each lifespan are reported in **Supplemental Data 7**.

665 Positive phototaxis assay: Statistical significance for phototaxis index at each timepoint
666 were calculated with the Student's *t*test (two-tailed, un-paired). 2way ANOVA or mixed-
667 effects models were performed to determine statistical significance between diet,
668 genotype, or time interactions. Full statistical output (2way ANOVA and *t*test) for all
669 phototaxis experiments is reported in **Supplemental Data 9**.
670 Real time quantitative PCR: Fold-change in gene expression was calculated using the ΔΔCt
671 method and the values were normalized using *rp49* as an internal control. *P*values were
672 calculated with the pairwise Student's *t*-test comparing Log2 fold-changes in expression.
673 Mass-spectrometric data processing, quantification and bioinformatics: Mass
674 spectrometric data-dependent acquisitions [51] were analyzed using the database search
675 engine ProteinPilot (SCIEX 5.0 revision 4769) using the Paragon algorithm (5.0.0.0,4767).
676 Using these database search engine results a MS/MS spectral library was generated in
677 Spectronaut 14.2.200619.47784 (Biognosys). The DIA/SWATH data was processed for
678 relative quantification comparing peptide peak areas from various different time points
679 during the cell cycle. For the DIA/SWATH MS2 data sets quantification was based on XICs
680 of 6-10 MS/MS fragment ions, typically y- and b-ions, matching to specific peptides
681 present in the spectral libraries. Peptides were identified at Q< 0.01%, significantly
682 changed proteins were accepted at a 5% FDR (*q*-value < 0.01).
683 Gene-ontology enrichment analysis: To identify enriched gene-ontology (i.e., bioprocess)
684 categories with the resultant lists from bioinformatics approaches, we utilized the

"findGO.pl" package from HOMER. Full gene-ontology lists including enrichment statistics and associated gene-lists are reported in supplemental data files. A maximal limit of 200 gene identifiers per GO category was implemented to reduce the occurrence of large, over-represented terms that lack specificity (i.e., *metabolism*). Full gene-ontology lists are reported in supplemental data files.

Data availability

Time-course microarray data and accompanied JTK_CYCLE statistics that support the findings in this study have been deposited in the Gene Expression Omnibus [74] with the GSE158286 accession code. The RNAseq data and accompanied differential expression analyses that support the findings in this study have been deposited to GEO with the GSE158905 accession code. The mass spectrometric raw data are deposited at ftp://MSV000086781@massive.ucsd.edu (MassIVE user ID: MSV000086781, password: winter; preferred engine: Firefox); it is also available at ProteomeXchange with the ID PXD023896. Additional mass spectrometric details from DIA and DDA acquisitions, such as protein identification and quantification details are available at the repositories (including all generated Spectronaut and Protein Pilot search engine files).

705

706

707

708

709

710

711

712

References

1. Rijo-Ferreira, F. and J.S. Takahashi, *Genomics of circadian rhythms in health and disease.* Genome Med, 2019. **11**(1): p. 82.
2. Patke, A., M.W. Young, and S. Axelrod, *Molecular mechanisms and physiological importance of circadian rhythms.* Nat Rev Mol Cell Biol, 2020. **21**(2): p. 67-84.
3. Rouyer, F., *Clock genes: from Drosophila to humans.* Bull Acad Natl Med, 2015. **199**(7): p. 1115-1131.
4. Ogueta, M., R.C. Hardie, and R. Stanewsky, *Non-canonical Phototransduction Mediates Synchronization of the Drosophila melanogaster Circadian Clock and Retinal Light Responses.* Curr Biol, 2018. **28**(11): p. 1725-1735 e3.
5. Hall, H., et al., *Transcriptome profiling of aging Drosophila photoreceptors reveals gene expression trends that correlate with visual senescence.* BMC Genomics, 2017. **18**(1): p. 894.
6. Lin, J.B., K. Tsubota, and R.S. Apte, *A glimpse at the aging eye.* NPJ Aging Mech Dis, 2016. **2**: p. 16003.
7. Felder-Schmittbuhl, M.P., et al., *Ocular Clocks: Adapting Mechanisms for Eye Functions and Health.* Invest Ophthalmol Vis Sci, 2018. **59**(12): p. 4856-4870.
8. Baba, K. and G. Tosini, *Aging Alters Circadian Rhythms in the Mouse Eye.* J Biol Rhythms, 2018. **33**(4): p. 441-445.
9. Kapahi, P., M. Kaeberlein, and M. Hansen, *Dietary restriction and lifespan: Lessons from invertebrate models.* Ageing Res Rev, 2017. **39**: p. 3-14.
10. Katewa, S.D., et al., *Peripheral Circadian Clocks Mediate Dietary Restriction-Dependent Changes in Lifespan and Fat Metabolism in Drosophila.* Cell Metab, 2016. **23**(1): p. 143-54.
11. Eckel-Mahan, K.L., et al., *Reprogramming of the circadian clock by nutritional challenge.* Cell, 2013. **155**(7): p. 1464-78.
12. Honma, T., et al., *High-fat diet intake accelerates aging, increases expression of Hsd11b1, and promotes lipid accumulation in liver of SAMP10 mouse.* Biogerontology, 2012. **13**(2): p. 93-103.
13. Montell, C., *Visual transduction in Drosophila.* Annu Rev Cell Dev Biol, 1999. **15**: p. 231-68.
14. Montell, C., *Drosophila visual transduction.* Trends Neurosci, 2012. **35**(6): p. 356-63.
15. Kuintzle, R.C., et al., *Circadian deep sequencing reveals stress-response genes that adopt robust rhythmic expression during aging.* Nat Commun, 2017. **8**: p. 14529.
16. Spitschan, M., et al., *Variation of outdoor illumination as a function of solar elevation and light pollution.* Sci Rep, 2016. **6**: p. 26756.
17. Gu, Y., et al., *Mechanisms of light adaptation in Drosophila photoreceptors.* Curr Biol, 2005. **15**(13): p. 1228-34.
18. Oberwinkler, J. and D.G. Stavenga, *Calcium transients in the rhabdomeres of dark- and light-adapted fly photoreceptor cells.* J Neurosci, 2000. **20**(5): p. 1701-9.
19. Shieh, B.H., *Molecular genetics of retinal degeneration: A Drosophila perspective.* Fly (Austin), 2011. **5**(4): p. 356-68.

20. Voolstra, O. and A. Huber, *Ca(2+) Signaling in Drosophila Photoreceptor Cells.* Adv Exp Med Biol, 2020. **1131**: p. 857-879.
21. Katewa, S.D. and P. Kapahi, *Dietary restriction and aging, 2009.* Aging Cell, 2010. **9**(2): p. 105-12.
22. Hotta, Y. and S. Benzer, *Abnormal electroretinograms in visual mutants of Drosophila.* Nature, 1969. **222**(5191): p. 354-6.
23. Vilinsky, I. and K.G. Johnson, *Electroretinograms in Drosophila: a robust and genetically accessible electrophysiological system for the undergraduate laboratory.* J Undergrad Neurosci Educ, 2012. **11**(1): p. A149-57.
24. Garschall, K. and T. Flatt, *The interplay between immunity and aging in Drosophila.* F1000Res, 2018. **7**: p. 160.
25. Pletcher, S.D., et al., *Genome-wide transcript profiles in aging and calorically restricted Drosophila melanogaster.* Curr Biol, 2002. **12**(9): p. 712-23.
26. Ferrandon, D., et al., *The Drosophila systemic immune response: sensing and signalling during bacterial and fungal infections.* Nat Rev Immunol, 2007. **7**(11): p. 862-74.
27. Handke, B., et al., *The hemolymph proteome of fed and starved Drosophila larvae.* PLoS One, 2013. **8**(6): p. e67208.
28. Palladino, M.J., et al., *Neural dysfunction and neurodegeneration in Drosophila Na+/K+ ATPase alpha subunit mutants.* J Neurosci, 2003. **23**(4): p. 1276-86.
29. Baumann, O., *Distribution of Na+,K(+)-ATPase in photoreceptor cells of insects.* Int Rev Cytol, 1997. **176**: p. 307-48.
30. Damulewicz, M., E. Rosato, and E. Pyza, *Circadian regulation of the Na+/K+-ATPase alpha subunit in the visual system is mediated by the pacemaker and by retina photoreceptors in Drosophila melanogaster.* PLoS One, 2013. **8**(9): p. e73690.
31. Luan, Z., K. Reddig, and H.S. Li, *Loss of Na(+)/K(+)-ATPase in Drosophila photoreceptors leads to blindness and age-dependent neurodegeneration.* Exp Neurol, 2014. **261**: p. 791-801.
32. Wijnen, H., et al., *Control of daily transcript oscillations in Drosophila by light and the circadian clock.* PLoS Genet, 2006. **2**(3): p. e39.
33. Kumar, J.P., *Building an ommatidium one cell at a time.* Dev Dyn, 2012. **241**(1): p. 136-49.
34. Wang, T. and C. Montell, *Phototransduction and retinal degeneration in Drosophila.* Pflugers Arch, 2007. **454**(5): p. 821-47.
35. Kurada, P. and J.E. O'Tousa, *Retinal degeneration caused by dominant rhodopsin mutations in Drosophila.* Neuron, 1995. **14**(3): p. 571-9.
36. Li, Q., et al., *Temperature and Sweet Taste Integration in Drosophila.* Curr Biol, 2020. **30**(11): p. 2051-2067 e5.
37. Vasiliauskas, D., et al., *Feedback from rhodopsin controls rhodopsin exclusion in Drosophila photoreceptors.* Nature, 2011. **479**(7371): p. 108-12.
38. Leung, N.Y., et al., *Functions of Opsins in Drosophila Taste.* Curr Biol, 2020. **30**(8): p. 1367-1379 e6.
39. Shostal, O.A. and A.A. Moskalev, *The genetic mechanisms of the influence of the light regime on the lifespan of Drosophila melanogaster.* Front Genet, 2012. **3**: p. 325.

40. Nash, T.R., et al., *Daily blue-light exposure shortens lifespan and causes brain neurodegeneration in Drosophila.* NPJ Aging Mech Dis, 2019. **5**: p. 8.
41. Ferreiro, M.J., et al., *Drosophila melanogaster White Mutant w(1118) Undergo Retinal Degeneration.* Front Neurosci, 2017. **11**: p. 732.
42. Yoon, J., et al., *Novel mechanism of massive photoreceptor degeneration caused by mutations in the trp gene of Drosophila.* J Neurosci, 2000. **20**(2): p. 649-59.
43. Scott, K., et al., *Gq alpha protein function in vivo: genetic dissection of its role in photoreceptor cell physiology.* Neuron, 1995. **15**(4): p. 919-27.
44. Shieh, B.H., I. Kristaponyte, and Y. Hong, *Distinct roles of arrestin 1 protein in photoreceptors during Drosophila development.* J Biol Chem, 2014. **289**(26): p. 18526-34.
45. Satoh, A.K. and D.F. Ready, *Arrestin1 mediates light-dependent rhodopsin endocytosis and cell survival.* Curr Biol, 2005. **15**(19): p. 1722-33.
46. Klapoetke, N.C., et al., *Independent optical excitation of distinct neural populations.* Nat Methods, 2014. **11**(3): p. 338-46.
47. Simpson, J.H. and L.L. Looger, *Functional Imaging and Optogenetics in Drosophila.* Genetics, 2018. **208**(4): p. 1291-1309.
48. Dolph, P.J., et al., *An eye-specific G beta subunit essential for termination of the phototransduction cascade.* Nature, 1994. **370**(6484): p. 59-61.
49. Stahl, A.L., et al., *The cuticular nature of corneal lenses in Drosophila melanogaster.* Dev Genes Evol, 2017. **227**(4): p. 271-278.
50. Kryuchkov, M., et al., *Reverse and forward engineering of Drosophila corneal nanocoatings.* Nature, 2020. **585**(7825): p. 383-389.
51. Xu, H., et al., *A lysosomal tetraspanin associated with retinal degeneration identified via a genome-wide screen.* EMBO J, 2004. **23**(4): p. 811-22.
52. Abruzzi, K.C., et al., *Drosophila CLOCK target gene characterization: implications for circadian tissue-specific gene expression.* Genes Dev, 2011. **25**(22): p. 2374-86.
53. Patel, S.A., et al., *Circadian clocks govern calorie restriction-mediated life span extension through BMAL1- and IGF-1-dependent mechanisms.* FASEB J, 2016. **30**(4): p. 1634-42.
54. Giebultowicz, J.M. and D.M. Long, *Ageing and Circadian rhythms.* Curr Opin Insect Sci, 2015. **7**: p. 82-86.
55. Hood, S. and S. Amir, *The aging clock: circadian rhythms and later life.* J Clin Invest, 2017. **127**(2): p. 437-446.
56. Boomgarden, A.C., et al., *Chronic circadian misalignment results in reduced longevity and large-scale changes in gene expression in Drosophila.* BMC Genomics, 2019. **20**(1): p. 14.
57. Martinez-Nicolas, A., et al., *Circadian monitoring as an aging predictor.* Sci Rep, 2018. **8**(1): p. 15027.
58. Retaux, S. and D. Casane, *Evolution of eye development in the darkness of caves: adaptation, drift, or both?* Evodevo, 2013. **4**(1): p. 26.
59. Lang, S., et al., *A conserved role of the insulin-like signaling pathway in diet-dependent uric acid pathologies in Drosophila melanogaster.* PLoS Genet, 2019. **15**(8): p. e1008318.

60. Nicholson, L., et al., *Spatial and temporal control of gene expression in Drosophila using the inducible GeneSwitch GAL4 system. I. Screen for larval nervous system drivers.* Genetics, 2008. **178**(1): p. 215-34.
61. Katewa, S.D., et al., *Intramyocellular fatty-acid metabolism plays a critical role in mediating responses to dietary restriction in Drosophila melanogaster.* Cell Metab, 2012. **16**(1): p. 97-103.
62. Bolger, A.M., M. Lohse, and B. Usadel, *Trimmomatic: a flexible trimmer for Illumina sequence data.* Bioinformatics, 2014. **30**(15): p. 2114-20.
63. Kim, D., B. Langmead, and S.L. Salzberg, *HISAT: a fast spliced aligner with low memory requirements.* Nat Methods, 2015. **12**(4): p. 357-60.
64. Liao, Y., G.K. Smyth, and W. Shi, *featureCounts: an efficient general purpose program for assigning sequence reads to genomic features.* Bioinformatics, 2014. **30**(7): p. 923-30.
65. Love, M.I., W. Huber, and S. Anders, *Moderated estimation of fold change and dispersion for RNA-seq data with DESeq2.* Genome Biol, 2014. **15**(12): p. 550.
66. Wang, S., et al., *The retromer complex is required for rhodopsin recycling and its loss leads to photoreceptor degeneration.* PLoS Biol, 2014. **12**(4): p. e1001847.
67. Wes, P.D., et al., *Termination of phototransduction requires binding of the NINAC myosin III and the PDZ protein INAD.* Nat Neurosci, 1999. **2**(5): p. 447-53.
68. Vang, L.L., A.V. Medvedev, and J. Adler, *Simple ways to measure behavioral responses of Drosophila to stimuli and use of these methods to characterize a novel mutant*. PLoS One, 2012. **7**(5): p. e37495.
69. Christensen, D.G., et al., *Identification of Novel Protein Lysine Acetyltransferases in Escherichia coli.* mBio, 2018. **9**(5).
70. Collins, B.C., et al., *Multi-laboratory assessment of reproducibility, qualitative and quantitative performance of SWATH-mass spectrometry.* Nat Commun, 2017. **8**(1): p. 291.
71. Schilling, B., B.W. Gibson, and C.L. Hunter, *Generation of High-Quality SWATH((R)) Acquisition Data for Label-free Quantitative Proteomics Studies Using TripleTOF((R)) Mass Spectrometers.* Methods Mol Biol, 2017. **1550**: p. 223-233.
72. Charlton-Perkins, M.A., et al., *Multifunctional glial support by Semper cells in the Drosophila retina.* PLoS Genet, 2017. **13**(5): p. e1006782.
73. Hughes, M.E., J.B. Hogenesch, and K. Kornacker, *JTK_CYCLE: an efficient nonparametric algorithm for detecting rhythmic components in genome-scale data sets.* J Biol Rhythms, 2010. **25**(5): p. 372-80.
74. Hardie, R.C., et al., *Molecular basis of amplification in Drosophila phototransduction: roles for G protein, phospholipase C, and diacylglycerol kinase.* Neuron, 2002. **36**(4): p. 689-701.

Acknowledgements

We would like to thank the QB3 Genomics Functional Genomics Lab at UC Berkeley and the Vincent J. Coates Genomics Sequencing Lab for RNA-seq library preparation and deep sequencing. We thank the Bloomington *Drosophila* Stock Center, the Vienna *Drosophila* Resource Center, and Craig Montell for providing flies used in this study. We would like to acknowledge Hugo Bellen and Zhongyuan Zuo for contributing resources and insight. We thank Daron Yim and John McCarthy for their assistance. We would like to acknowledge the work of Paolo Sassone-Corsi and his recent contributions to the fields on nutrition, circadian rhythms, and aging that helped in the conception of this project.

This work is funded by grants awarded to P.K. from the American Federation of Aging Research, NIH grants R01 R01AG038688 and AG045835 and the Larry L. Hillblom Foundation. B.A.H. is supported by NIH/NIA T32 award AG000266 and C.M. is supported by NIH/NEI awards EY008117 and EY010852. We acknowledge the Buck Institute Proteomics Core and the support of instrumentation from the NCRR shared instrumentation grant 1S10 OD016281.

Author Contributions

Conceptualization, B.A.H., G.T.M., and S.K.; Software, B.A.H., G.T.M., B.S., and S.K.; Formal analysis, B.A.H., G.T.M., and B.S.; Investigation, B.A.H., G.T.M., C.L., T.L., N.L., D.L-K., and S.B.;

Visualization, B.A.H.; Writing-Original Draft, B.A.H., Writing-Review & Editing, B.A.H., G.T.M., and P.K.; Data Curation, B.A.H., G.T.M., S.M., and B.S.; Methodology, G.T.M. and M.L., Resources, C.M. and P.K., Supervision, P.K., Funding acquisition, C.M. and P.K.

Additional information

The authors declare no competing interests.

Supplementary Information is available for this paper

Correspondence and requests for materials should be addressed to
P.K. (pkapahi@buckinstitute.org)

Supplementary Files

This is a list of supplementary files associated with this preprint. Click to download.

- Supplemental.pdf
- SupplementalData1.xlsx
- SupplementalData2.xlsx
- SupplementalData3.xlsx
- SupplementalData4.xlsx
- SupplementalData5.xlsx
- SupplementalData6.xlsx
- SupplementalData7.xlsx
- SupplementalData8.xlsx
- SupplementalData9.xlsx
- SupplementalData10.xlsx
- SupplementalData11.xlsx